ChemCatChem

Research Article
doi.org/10.1002/cctc.202301358

Chemistry Europe
European Chemical Societies Publishing

www.chemcatchem.org

TiO_2–CeO_x–Pt Hollow Nanosphere Catalyst for Low-Temperature CO Oxidation

Mareike Liebertseder,[a] Carina B. Maliakkal,[b] Marlene Crone,[c] Gülperi Nails,[d] Maria Casapu,[d] Jan-Dierk Grunwaldt,[d, e] Michael Türk,[c] Christian Kübel,[b] and Claus Feldmann*[a]

TiO_2–CeO_2–Pt hollow nanospheres (1 wt-% Pt) are realized using a liquid-phase strategy using NaCl as a template. The NaCl template is first coated with TiO_2 and thereafter with CeO_2 via the hydrolyzation of $TiCl(OiPr)_3$ and $Ce(OiPr)_4$ as suitable alkoxides. Finally, the NaCl template is removed by washing with water. The resulting @TiO_2–CeO_2 hollow nanospheres (□: inner cavity) exhibit an outer diameter of 140–180 nm, a wall thickness of 30–40 nm, an inner cavity of 80–100 nm, a specific surface area of 210 m^2/g, a pore volume and area of 0.08 cm^3/g and 191 m^2/g, mainly with micropores $\geq$5 Å and $\leq$14 Å. The hollow nanosphere support is impregnated with Pt nanoparticles, using two different methods – a wet-chemical deposition ($Pt(ac)_2$, acetone, 25 °C) and a supercritical fluid reactive deposition (SFRD) process ([Pt(COD)Me_2], supercritical CO_2, 80 °C, 15.6 MPa) resulting in an uniform size distribution with Pt nanoparticles 2.5 ± 0.1 nm (TiO_2–CeO_2–Pt_{WCD}) and 2.3 ± 0.1 nm (TiO_2–CeO_2–Pt_{SFRD}) in size. The catalytic properties of the TiO_2–CeO_2–Pt hollow nanospheres are evaluated for CO oxidation between 50 and 500 °C. A promising catalytic activity and stable light-out/light-off temperatures are observed especially for the TiO_2–CeO_2–Pt_{SFRD} sample, indicating the suitability of hollow nanospheres as high-porosity catalyst material.

Introduction

Ceria belongs to the most relevant support materials for heterogeneous catalysis.[1] Particularly important, for instance, are emission control,[2] reverse water gas shift, electrocatalysis and fuel cells,[3] direct synthesis of H_2O_2,[4] or – as a related topic – the detection of combustible gases.[5] In combination with a precious metal, which is essential to catalyze the corresponding redox reaction, ceria as the support contributes to the catalytic reaction via perimeter sites at the noble-metal to oxide-support interface. Oxygen at the interface can be provided in a Mars-van-Krevelen-like mechanism to oxidize CO adsorbed on the precious metal.[1,6] In regard of such heterogeneous catalytic reactions, a high surface area of the ceria support and small-sized precious metal particles homogeneously distributed over the ceria surface are prerequisites to a high number of active surface sites and a high activity of the composite catalyst. To this concern, various nanocomposite catalysts have been suggested, including multicomponent compositions and elaborate nanostructures.[1–6]

Ceria crystallizes in the calcium-fluorite-type structure and is well-kown for good oxide-ion conductivity at elevated temperature (>200 °C).[7] While this fast diffusion is advantageous in regard of the oxygen storage of the composite catalyst to balance the oxygen concentration during the catalytic reaction, the oxide-ion conductivity can be disadvantageous in regard of the thermal stability of the composite catalyst.[1,7] Thus, the ion mobility promotes sintering of ceria, which can cause a temperature- and time-dependent decrease of the surface area as well as a reduction or even vanishing of small pores and reactive surface sites. In addition, ion conductivity and sintering of the support can lead to a higher mobility of metal nanoparticles on the support surface, which then also can agglomerate, increase in size and loose catalytic activity.[8]

Hollow nanospheres are generally known for their high surface area in combination with high mechanical stability.[9] In the case of ceria, hollow nanospheres as catalyst supports have been prepared via template-based approaches, for instance,

[a] Dr. M. Liebertseder, Prof. Dr. C. Feldmann
Institute of Inorganic Chemistry (IAC)
Karlsruhe Institute of Technology (KIT)
Engesserstraße 15, D-76131 Karlsruhe (Germany)
E-mail: claus.feldmann@kit.edu

[b] Dr. C. B. Maliakkal, Prof. Dr. C. Kübel
Institute of Nanotechnology (INT) and Karlsruhe Nano Micro Facility (KNMFi)
Karlsruhe Institute of Technology (KIT)
Hermann-von-Helmholtz-Platz 1, 76344 Eggenstein-Leopoldshafen (Germany)

[c] M. Crone, Prof. Dr. M. Türk
Institute for Technical Thermodynamics and Refrigeration
Karlsruhe Institute of Technology (KIT)
Engler-Bunte-Ring 21, 76131 Karlsruhe (Germany)

[d] Dr. G. Nails, Dr. M. Casapu, Prof. Dr. J.-D. Grunwaldt
Institute for Chemical Technology and Polymer Chemistry (ITCP)
Karlsruhe Institute of Technology (KIT)
Engesserstraße 20, 76131 Karlsruhe (Germany)

[e] Prof. Dr. J.-D. Grunwaldt
Institute of Catalysis Research and Technology (IKFT)
Karlsruher Institute of Technology (KIT)
Hermann-von-Helmholtz-Platz 1, 76344 Eggenstein-Leopoldshafen (Germany)

Supporting information for this article is available on the WWW under https://doi.org/10.1002/cctc.202301358

with C_3N_4, Au, ZrO_2, Mn_3O_4, SiO_2, or polymers as a templates.[10] Alternative synthesis methods are based on Kirkendahl ripening, layer-by-layer deposition, or spray pyrolysis.[11] Beside catalysis, CeO_2 hollow nanospheres also turned out to be promising for photocatalytic CO reduction or as components for supercapacitors, lithium-sulfur batteries, and lithium-ion batteries.[10a,12] As a general limitation, the yet reported ceria hollow nanospheres often suffer from large particle diameters (>500 nm), comparably small surface areas (<100 m^2/g), and limited thermal stability (partially not even studied). As a new strategy and material addressing the needs of high-surface ceria with good thermal stability, we here suggest a one-pot synthesis of Pt-impregnated TiO_2–CeO_2 hollow nanospheres. They were prepared in a liquid-phase approach starting with NaCl templates, which were coated first with a TiO_2 shell, then with a CeO_2 shell, before the NaCl core was removed by dissolution in water. Finally, the TiO_2–CeO_2 hollow nanospheres were decorated with Pt nanoparticles using either a wet-chemical deposition (WCD) or via supercritical fluid reactive deposition (SFRD) in supercritical CO_2. The as-obtained TiO_2–CeO_2–Pt hollow nanospheres were evaluated in CO oxidation as test reaction.

Results and Discussion

Synthesis of TiO_2–CeO_2–Pt hollow nanospheres

TiO_2–CeO_2–Pt hollow nanospheres were prepared in a one-pot approach in the liquid phase via a modified synthesis protocol as we recently reported for TiO_2 hollow nanosphere supports.[13] Here, it should be noticed that all our attempts to directly realize stable CeO_2 hollow nanosphere supports failed so far. This can be attributed to the significantly lower mechanical and especially the lower thermal stability of CeO_2 hollow spheres in comparison to TiO_2 hollow nanospheres.

The most essential aspect of our synthesis strategy relates to the formation of NaCl nanoparticles as a template, which – after the deposition of the TiO_2 and CeO_2 shells – can be easily removed by washing with water (Figure 1). To obtain NaCl nanoparticles, a solvent-antisolvent approach was used.[13] Thus, a saturated solution of NaCl in methanol (MeOH) as the solvent was injected into tetrahydrofuran (THF) as the antisolvent. Whereas NaCl is well-soluble in MeOH, it is insoluble in THF. Upon injection of the NaCl solution, immediate nucleation of NaCl occurred, resulting in crystalline, cube-like NaCl nanoparticles, 80–100 nm in diameter (Figure 1a). As a next step, a TiO_2 shell was deposited on the NaCl template upon slow addition and hydrolysis of $TiCl(OiPr)_3$. Previous studies have shown that this step requires special attention in order to realize a uniform TiO_2 shell on the NaCl template.[13] Most important is a tiny portion of water to be added to the NaCl template prior to the alkoxide to promote beginning hydrolysis and titania formation on the NaCl surface. As a result, NaCl@TiO_2 core@shell nanoparticles with a TiO_2 shell, 30–40 nm in thickness are formed (Figure 1b).

Subsequent to the formation of the TiO_2 shell, the ceria shell is established in a similar way. Here, $Ce(OiPr)_4$[14] was added as a cerium alkoxide and again slowly hydrolyzed to obtain a NaCl@TiO_2–CeO_2 core@shell structure (Figure 1c). The hydrolysis was performed with diluted H_2O_2 to guarantee the presence of Ce^{4+} and to avoid Ce^{3+}. Finally, the NaCl template was removed from the particle core by washing with water. The solubility of NaCl from the inner particle core already points to the presence of pores through the wall of the TiO_2@CeO_2 hollow nanospheres. Such pores are anyway needed for catalysis and also lead to a further increase of the pore volume and the surface area in addition to the outer surface and the surface of the inner cavity of the hollow nanospheres. In sum, the resulting

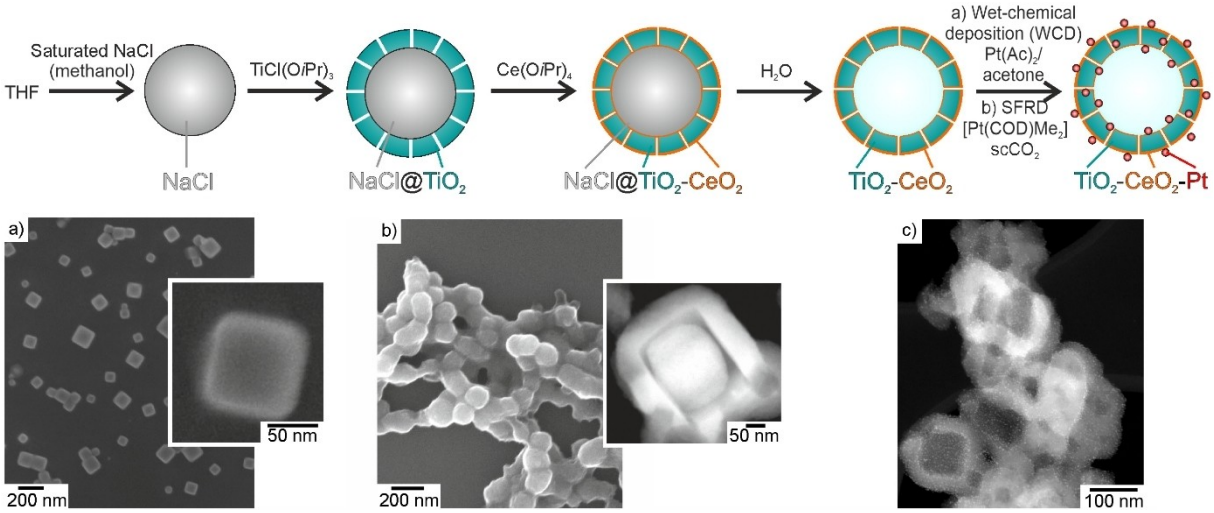

Figure 1. Synthesis of □@TiO_2–CeO_2–Pt core@shell hollow nanosphere catalyst with scheme of synthesis strategy and a-c) exemplary electron microscopy images of NaCl template (a), NaCl@TiO_2 core@shell nanoparticles (b),[13] and □@TiO_2–CeO_2–Pt core@shell hollow nanospheres (□ indicating the inner cavity left after removal of the NaCl template) after Pt impregnation either via wet-chemical deposition (WCD) or supercritical fluid reactive deposition (SFRD) process (c).

metal-oxide support could be designated as □@TiO_2–CeO_2 core@shell hollow nanospheres with indicating the inner cavity (the former NaCl template).

Impregnation of TiO_2–CeO_2 hollow nanospheres with Pt

Two different strategies were applied to decorate the TiO_2–CeO_2 hollow nanosphere supports with Pt nanoparticles. This includes a wet-chemical deposition as well as a deposition in supercritical CO_2 ($scCO_2$) via the SFRD process (Figure 1c). The two different strategies were evaluated for two reasons. On the one hand, Pt is the active catalytic site for CO oxidation, so that the size of the Pt nanoparticles, their distribution over the support surface and the stability of the Pt nanoparticles are essential in regard of the catalytic activity. On the other hand, TiO_2–CeO_2 hollow nanospheres represent a new type of a catalyst support, so that establishing an efficient process for impregnation with Pt is relevant anyway.

As a first process, the TiO_2–CeO_2 support was impregnated with Pt nanoparticles (1 wt-%) via a wet-chemical deposition (designated as TiO_2–CeO_2–Pt_{WCD}). To this concern, a solution of $Pt(Ac)_2$ in acetone was slowly dropped on a powder sample of the hollow nanospheres. Due to the low surface tension of acetone the $Pt(Ac)_2$ solution was instantaneously distributed over the support surface via capillary forces. Thereafter, the as-deposited $Pt(Ac)_2$ was reduced by reducing gas (N_2:H_2 = 10:90) already at room temperature (25 °C). Due to the fine dispersion of $Pt(Ac)_2$ over the porous TiO_2–CeO_2 prior to the reduction, a homogeneous distribution of small Pt nanoparticles is achieved. As a result, a uniform distribution of small Pt particles was achieved with 1 wt-% of Pt and a particle size of 2–3 nm. This procedure was preferred over the more often used aqueous solutions of platinum chloride or platinum nitrate.[15] The latter requires certain heating for reduction (100–300 °C), which, however, promotes particle growth and leads to larger Pt nanoparticles than the here applied reduction at room temperature.

The supercritical fluid reactive deposition (SFRD) process already turned out as efficient to impregnate metal-oxide supports with metal nanoparticles.[16] Thus, $scCO_2$ is known as low-toxic solvent with good solubility for many metalorganic compounds and high capillary forces for sufficient permeation of highly porous materials. The SFRD process was performed at 80 °C and 15.6 MPa CO_2 (see SI).[17] [$Pt(COD)Me_2$] was used as metalorganic precursor and first allowed to adsorb on the surface of the TiO_2–CeO_2 support. Upon addition of H_2, the precursor was reduced to elemental Pt, while the organic ligands were transformed to 1,5-cyclooctane and methane. Due to complete miscibility of $scCO_2$ with the hydrogenated ligands, residues solvent and reactants on the catalyst surface can be avoided after depressurization. As a result, a TiO_2–CeO_2–Pt_{SFRD} hollow nanospheres catalyst was obtained.

Size and structure of TiO_2–CeO_2 hollow nanospheres

First of all, the size and structure of the TiO_2–CeO_2 support were examined by electron microscopy and electron spectroscopy. Transmission electron microscopy (TEM) validates the hollow-sphere-type structure with an inner cube-shaped cavity of 80–100 nm in diameter, originating from the former NaCl template, and a solid shell with a wall thickness of 30–40 nm (Figure 2a). Overall, a rounded outer shape is observed with an outer diameter of 140–180 nm. Element mapping via scanning transmission electron microscopy (STEM) based on energy-dispersive X-ray spectroscopy (EDXS) indicates a uniform distribution of titanium and cerium all over the hollow nanospheres (Figure 2b–d). Interestingly, a thin CeO_2 layer is finely dispersed all over the TiO_2 hollow nanospheres, including the pores through the sphere wall as well as the inner cavity surface. This finding is especially confirmed by high-resolution images of the sphere wall (Figure 3). Finally, it should be noticed that no Na/Cl-related signals could be detected by EDXS element maps, which points to a complete removal of the NaCl template out of the TiO_2–CeO_2–Pt hollow nanospheres.

Physisorption analysis performed with N_2 as probe molecule evidences the porosity of the TiO_2–CeO_2 hollow nanospheres (Figure 4a). Accordingly, a specific surface area of 219 m^2/g was determined based on the Brunauer-Emmett-Teller (BET) formalism. Moreover, a pore volume and area of 0.08 cm^3/g and 191 m^2/g as well as an external surface area of 28 m^2/g were determined by the *t*-plot method (Supporting Information, Figure S1).[18] In regard of the pore diameter, predominately micropores ($\geq$ 5 Å and $\leq$ 14 Å) were observed (Figure 4b). With these values, the CeO_2-coated surface of the TiO_2–CeO_2 hollow nanospheres represents one of the greatest surface areas

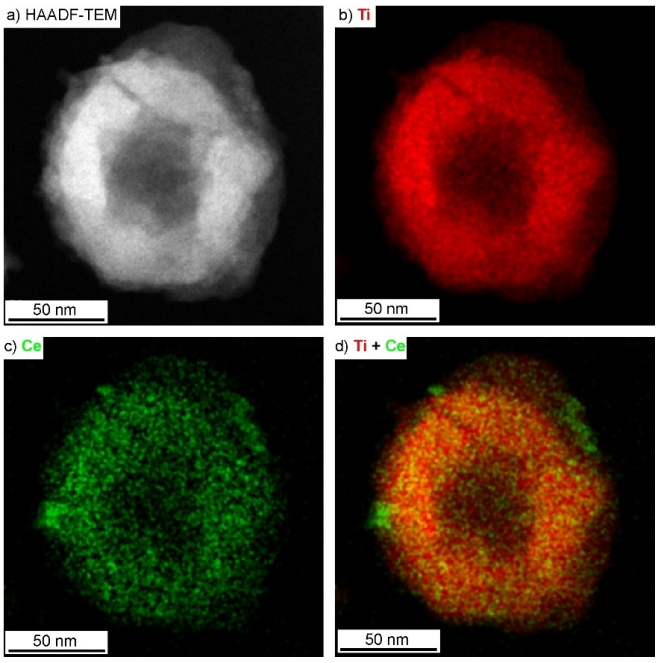

Figure 2. Size and structure of the TiO_2–CeO_2 hollow nanospheres: a) HAADF-STEM overview image, b)–d) EDXS element maps of Ti (b), Ce (c), Ti + Ce (d).

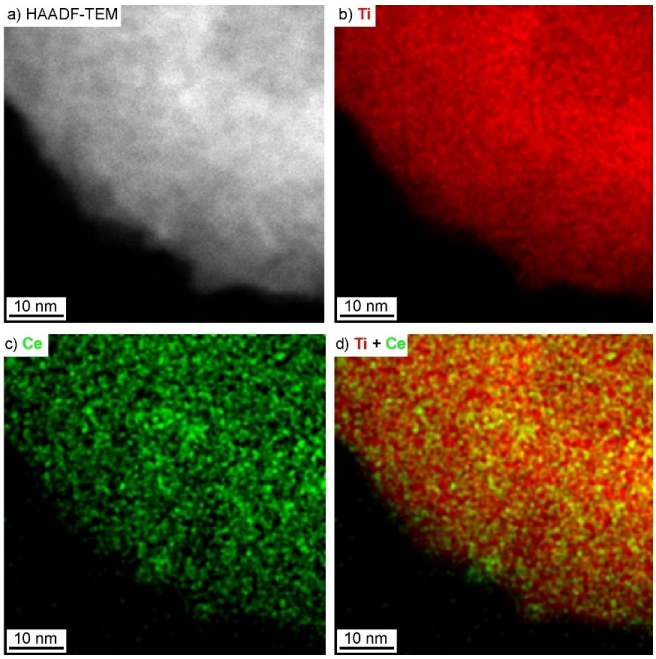

Figure 3. High-resolution images of the TiO_2–CeO_2 hollow nanospheres: a) HAADF-STEM overview image, b)–d) EDXS element maps of Ti (b), Ce (c), Ti + Ce (d).

reported for CeO_2. The highest specific surface area was yet reported with 100 m^2/g for mesoporous zirconia-ceria mixtures[19] or with 170 m^2/g for very small (3–5 nm) massive CeO_2 nanoparticles.[20] Higher values of 250 m^2/g were – to the best of our knowledge – only reported for microemulsion-made CeO_2 nanoparticles, which, however, generates very small amounts of material.[21] Previous studies on TiO_2 hollow spheres, already showed the hollow sphere support to be thermally stable up to 400 °C.[13] Thus, heating to 300 °C resulted in a reduction of the specific surface area of only about 10%, which is still high in comparison to literature data.[19–21] Here, it needs to be noticed that the thermal behavior of CeO_2 hollow spheres was partly not even studied in the literature.

Finally, X-ray powder diffraction was performed to verify composition and crystallinity of the TiO_2–CeO_2–Pt hollow nanospheres (Figure S2). The as-prepared TiO_2–CeO_2–Pt hollow nanospheres do not show any Bragg reflection, which is to be expected for the high-porosity catalyst. Even after heating to 400 °C, only TiO_2 in the anatase modification shows very broad Bragg reflections, which points to a high-porosity structure even after certain heating. Due to their low scattering power, the thin CeO_2 layer and the very small Pt nanoparticles still do not show any Bragg reflection (Figure S2). With temperatures $\geq$800 °C, Bragg reflections of TiO_2 (rutile modification), CeO_2 and Pt become visible. Although not being a porous nanomaterial anymore, the presence of TiO_2, CeO_2 and Pt after high-temperature sintering nevertheless evidences their presence also at lower temperature (Figure S2).

Size and structure of deposited Pt nanoparticles

Whereas structure and shape of the TiO_2–CeO_2 support are independent of the procedure chosen to deposit platinum, the size and distribution of the Pt nanoparticles over the support surface were studied in detail for the two different impregnation processes. To this concern, higher magnification STEM was used to elucidate size and distribution of the Pt nanoparticles on the hollow nanosphere support after wet-chemical deposition (Figure 5) and after the SFRD process (Figure 6). First of all, the spherical outer shape with the sphere wall and the cube-shaped inner cavity of the hollow nanosphere support are clearly visible on STEM images (Figures 5a, 6a).

For the wet-chemical impregnation process, a uniform distribution of Pt nanoparticles on the outer as well as on the inner surface of the TiO_2–CeO_2–Pt_{WCD} hollow nanospheres is displayed in EDXS element maps (Figure 5). Very small Pt nanoparticles with a mean diameter of 2.5 ± 0.1 nm are visible ($x_{50} \pm \sigma$, Figure 7). Herein, the polydispersity Δ was calculated by $\Delta = [(x_{90} - x_{10})/2\, x_{50}]$. The mean particle size x_{50} is defined as the diameter, at which 50% of the particles have a larger diameter and the other 50% have a smaller diameter (x_{10}, x_{90} defined accordingly). The Pt nanoparticles are finally almost equally distributed over the outer and inner surface of the hollow nanospheres (Figure 5a, d). For the Pt-nanoparticle impregnation using the SFRD process, representative TEM images again show a uniform decoration of Pt nanoparticles all over the TiO_2–CeO_2–Pt_{SFRD} hollow nanospheres (Figure 6). Again, very

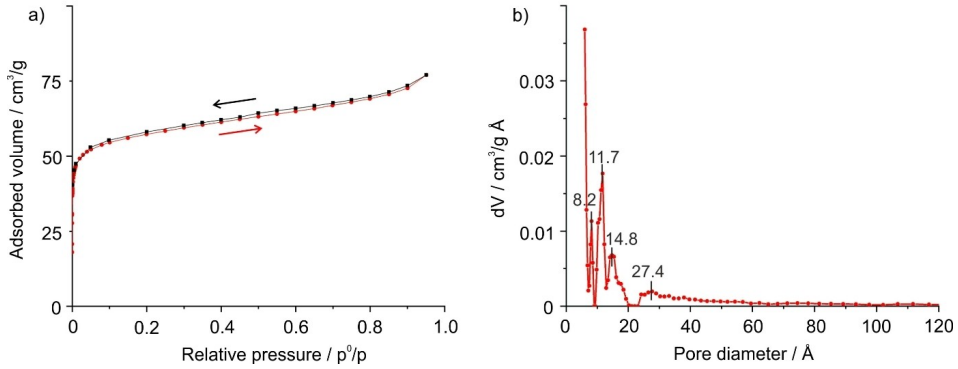

Figure 4. Surface area and pore volume of the TiO_2–CeO_2 hollow nanospheres: a) N_2-based sorption analysis, b) distribution of pore diameters.

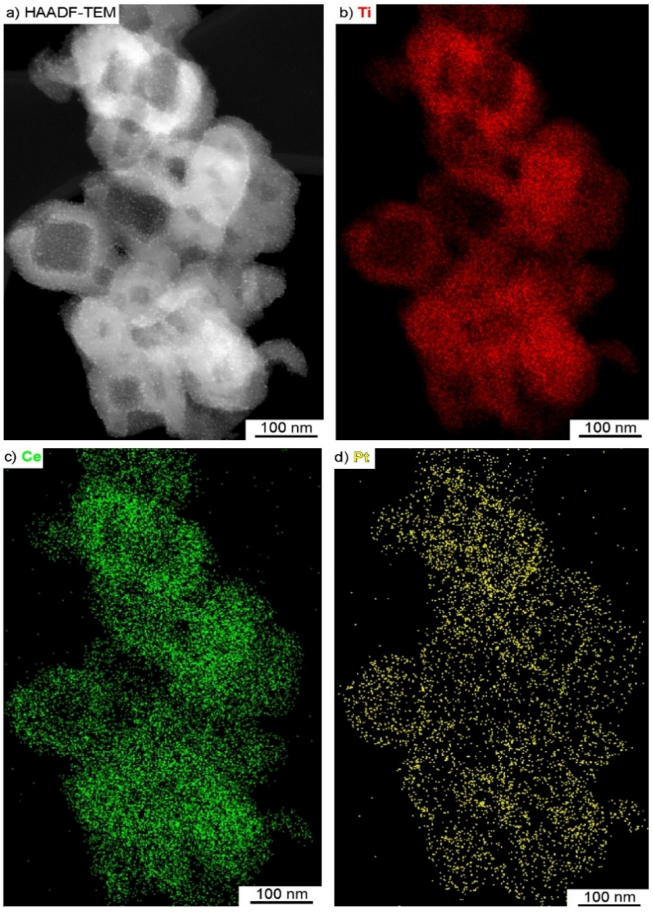

Figure 5. Size and structure of the TiO_2–CeO_2–Pt_{WCD} hollow nanospheres: a) HAADF-STEM image, b)–d) STEM-EDXS maps of Ti (red), O (blue), Ce (green), and Pt (yellow).

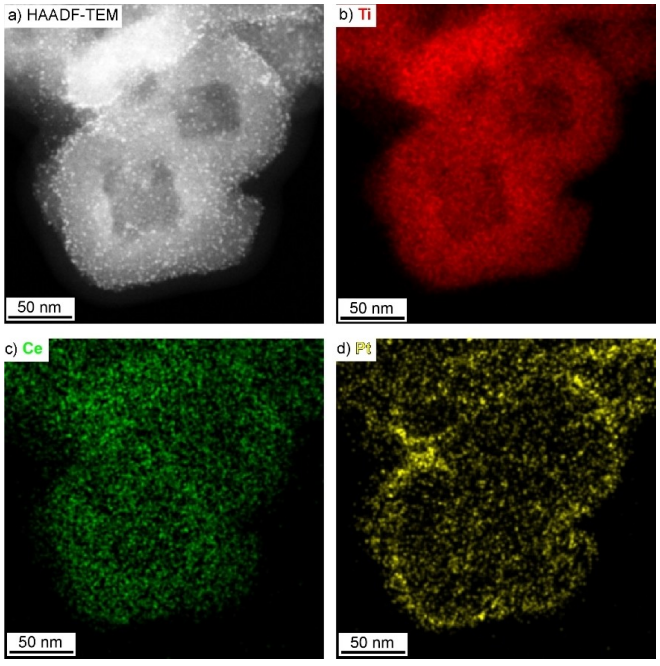

Figure 6. Size and structure of the TiO_2–CeO_2–Pt_{SFRD} hollow nanospheres: a) HAADF-STEM image, b)–d) STEM-EDXS maps of Ti (red), O (blue), Ce (green), and Pt (yellow).

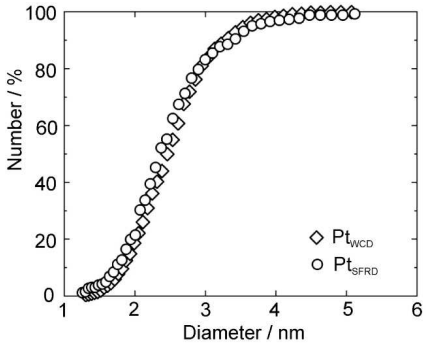

Figure 7. Size and size distribution of the Pt nanoparticles on TiO_2–CeO_2–Pt_{WCD} and TiO_2–CeO_2–Pt_{SFRD} hollow nanospheres.

small Pt nanoparticles were obtained with a mean diameter of 2.3 ± 0.1 nm ($x_{50} \pm \sigma$, Figure 7). In comparison to the wet-chemical deposition, the diameter of the Pt nanoparticles stemming from the SFRD process turned out to be slightly smaller. However, more Pt nanoparticles are located on the outer surface of the catalyst support as compared to the inner cavity surface (Figure 6a, d).

Catalytic activity of TiO_2–CeO_2–Pt hollow nanospheres

For the present study, the temperature range relevant for CO oxidation was investigated (i.e. up to 500 °C). CO conversion and catalyst stability were monitored during consecutive light-off/light-out cycles, while applying a ramp rate of 5 °C/min. In this way not only the initial activity was determined but also the performance after catalyst degreening under reaction conditions. The activity of CO oxidation was similarly tested for the TiO_2–CeO_2–Pt_{WCD} and TiO_2–CeO_2–Pt_{SFRD} catalysts during two consecutive light-off/light-out cycles (Figure 8) without any catalyst pre-treatment. Considering that both samples were exposed to ambient atmosphere prior to the catalytic tests, at least partial oxidation of the Pt nanoparticle surface is expected to occur despite both catalyst synthesis procedures involved a reductive step. Hence, CO oxidation is anticipated to occur only at temperatures sufficiently high for the reduction of Pt nanoparticles under reaction conditions.[22]

For the TiO_2–CeO_2–Pt_{WCD} sample, a relatively high light-off temperature (50 % of activity reached at 284 °C during heating) and a slow increase of the CO oxidation activity were observed during the 1st cycle (Figure 8a). In contrast, 100 % conversion was maintained during the cooling down step even at 210 °C, followed by a sharp decrease in activity and a light-out temperature of 200 °C (50 % of activity reached for the cooling cycle). Despite the reducing treatment (N_2:H_2 = 10:90) applied at 25 °C for the sample, this behavior can be ascribed to a certain catalyst degreening, including the removal of precursor traces and further crystallization of TiO_2 and CeO_2 during heating to 500 °C. Additionally, the noble metal state is expected to vary under reaction conditions due to the interaction with the CeO_2 support, leading to sintering/redispersion processes depending on the temperature and CO

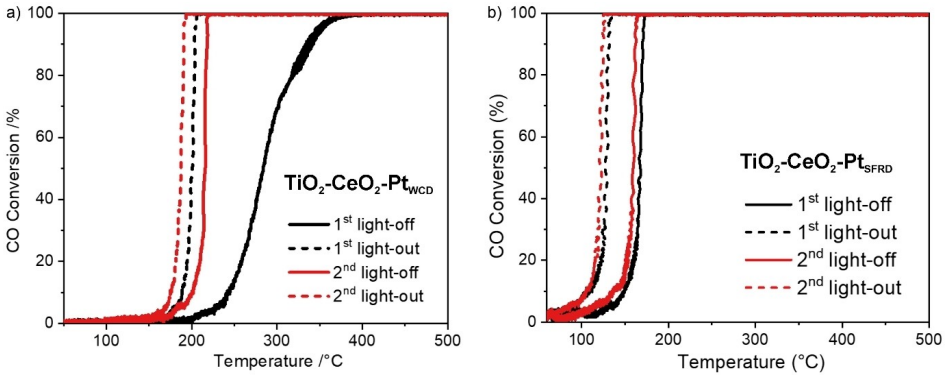

Figure 8. Results of CO oxidation activity tests for TiO_2–CeO_2 hollow nanospheres catalysts: a) TiO_2–CeO_2–Pt_{WCD}, b) TiO_2–CeO_2–Pt_{SFRD} (gas mixture: 50 mL/min of 1000 ppm CO, 10% O_2 in He; temperature ramp rate: 5 °C/min).

concentration.[6a] This improvement in activity and the steep CO oxidation profile is maintained also during the 2nd reaction cycle over the TiO_2–CeO_2–Pt_{WCD} hollow nanosphere catalyst. Moreover, in comparison to the 1st cycle, the light-off and light-out temperatures are very close in values (215 °C and 187 °C), showing a good catalyst stabilization. The appearance of a typical hysteresis between the light-off and light-out curves points to the presence of slightly larger Pt particles (>1 nm) as previously reported for alumina-supported catalysts.[23] However, the different CO oxidation mechanism involving perimeter sites at the interface between the noble metal and ceria support might contribute as well to the variation observed between the heating and cooling curves.[22] According to Artiglia *et al.*,[24] Ce^{3+} sites are generated at the interface between Pt and CeO_2 support and in the topmost layers of ceria during CO oxidation. This contribution helps overcoming the CO self-inhibition effect on Pt.[23,25]

For the TiO_2–CeO_2–Pt_{SFRD} catalyst, the two CO oxidation cycles are very similar in terms of the activity profile (Figure 8b). Light-off temperatures of 167 and 159 °C were recorded for the 1st and 2nd cycle, respectively. A slight activity improvement was measured also during the corresponding reaction light-outs with the temperatures of 50% conversion at 126 and 121 °C. This behavior is explained by the slightly smaller noble metal particle size and the narrow size distribution obtained during the SFRD-based deposition, which is less prone to major structural changes during the catalytic cycles. Also in this case the CO oxidation activity during cooling is higher as measured during the heating step, which is in line with the previously reported relation between Pt particle size and the shape of hysteresis loop.[26] Additionally, the location of the noble metal mainly on the outer cavity of the TiO_2–CeO_2 hollow nanospheres (Figure 6 *vs.* Figure 5) further explains the higher low-temperature activity of the TiO_2–CeO_2–Pt_{SFRD} catalyst in comparison to the TiO_2–CeO_2–Pt_{WCD} sample.

All in all, supplemented by further screening in catalyst composition (e.g., variation noble metal loading, testing under more realistic conditions and long-term durability tests), the promising potential of the new hollow-sphere material for catalytic applications as resulted from this study could be further exploited. Furthermore, the perspective of using such hierarchical structures on thermally stable supports, i.e. alumina, has been demonstrated previously as an efficient paths to prevent noble metal sintering due to strong noble metal interaction.[27]

Conclusions

TiO_2–CeO_2 hollow nanospheres as a metal-oxide support for catalytic CO oxidation are shown for the first time. They are prepared using NaCl nanoparticles as templates, which are sequentially coated by TiO_2 and, thereafter, by CeO_2. The NaCl template is prepared by a solvent-antisolvent approach by injecting a saturated solution of NaCl in water as the solvent into THF as the antisolvent. While water is soluble in THF, NaCl becomes insoluble and precipitates with formation of nanoparticles, 80–100 nm in size. The TiO_2 and CeO_2 shells are established by controlled hydrolysis of alkoxides ($TiCl(OiPr)_3$ and $Ce(OiPr)_4$). Thereafter, the NaCl template is removed simply by washing with water and resulting in TiO_2–CeO_2 hollow nanospheres with an outer diameter of 140–180 nm, a wall thickness of 30–40 nm, and an inner cavity of 80–100 nm. They exhibit a specific surface area of 210 m^2/g, a pore volume and area of 0.08 cm^3/g and 191 m^2/g as well as pores mainly in the 5 to 14 Å range. Finally, the TiO_2–CeO_2 hollow nanosphere support was impregnated with Pt nanoparticles using two different methods. On the one hand, a wet-chemical process is applied based on $Pt(Ac)_2$ in acetone and, on the other hand, a deposition via the SFRD process in supercritical CO_2 using $[Pt(COD)Me_2]$ as a precursor (COD: 1,5-cyclooctadiene, Me: methyl), which results in TiO_2–CeO_2–Pt_{WCD} and TiO_2–CeO_2–Pt_{SFRD} hollow nanosphere catalysts.

The resulting TiO_2–CeO_2–Pt hollow nanosphere catalysts exhibits a uniform distribution of Pt nanoparticles (1 wt-% Pt) with a size and size distribution of 2.5 ± 0.1 nm (WCD) and 2.3 ± 0.1 nm (SFRD). After some settling of the catalyst in the 1st reaction cycle, the TiO_2–CeO_2–Pt hollow nanosphere catalysts exhibit stable properties in the 2nd reaction cycle. TiO_2–CeO_2–Pt_{WCD} hollow nanospheres show only minor hysteresis between light-out and light-off but with slightly higher temperatures of 215 °C for light-off and 187 °C for light-out. In

contrast, TiO_2–CeO_2–Pt_{SFRD} hollow nanospheres show certain hysteresis even after the 2nd reaction cycle but with lower temperatures of 159 °C for light-off and 121 °C for light-out. In sum, TiO_2–CeO_2–Pt hollow nanosphere catalysts with a novel core@shell hollow nanosphere support show promising properties, which could be further enhanced with suitable material optimization. Moreover, the concept of NaCl templates to realize hollow nanosphere supports offers flexibility to realize other materials and catalysts.

Experimental Section

General. $TiCl(OiPr)_3$ (95 %, ABCR) was handled under inert gas conditions (glove boxes or Schlenk techniques). $Pt(ac)_2$ was prepared according to the literature.[28] Methanol (99 %, Seulberger) and NaCl (100 %, VWR Chemicals) were handled as purchased. Ethanol (99.9 %, Seulberger) was refluxed 3 days over Mg; THF (99 %, Seulberger) was refluxed 3 days over sodium and benzophenone. A saturated solution of NaCl in methanol was obtained by heating NaCl in methanol to 60 °C, followed by slow cooling and leaving the system for 12 hours at room temperature. Thereafter, the solution over the insoluble NaCl precipitate was saturated.

TiO_2–CeO_2 hollow nanospheres. 5 mL of a saturated solution of NaCl in methanol were injected into 120 mL of dried THF to obtain a suspension of NaCl nanoparticles following our previously published synthesis strategy.[13] Thereafter, 5 mL of a 0.1 M solution of $TiCl(OiPr)_3$ in ethanol were slowly added with a rate of 1 mL/h with a syringe pump. The alkoxide was hydrolyzed upon addition of 4 mL of H_2O, which were again added with a rate of 1 mL/h with a syringe pump. The resulting NaCl@TiO_2 core@shell nanoparticle suspension was stirred for additional 24 h, then centrifuged and the centrifugate resuspended again in 120 ml of dried THF.

As a next step, 5 mL of a solution of 0.01 M $Ce(OiPr)_4$ in THF were added with a rate of 1 mL/h with a syringe pump. Since $Ce(OiPr)_4$ was hardly available commercially with high purity, we have prepared ourselves by reacting cerium metal nanoparticles in dried isopropanol.[14] The alkoxide was hydrolyzed upon addition of 2 mL of 3 % aqueous H_2O_2. H_2O_2 was used to avoid any reduction of cerium to Ce^{3+}. Thereafter, the NaCl@TiO_2@CeO_2 core@shell nanoparticle suspension was stirred for additional 24 h. Thereafter, the nanoparticles were centrifuged and redispersed twice from/in ethanol and twice from/in water to remove all soluble salts and excess starting materials. Washing with water also leads to a dissolution of the inner NaCl core, so that □@TiO_2–CeO_2 core@shell nanoparticles – in the following designated as TiO_2–CeO_2 hollow nanospheres – were formed. Finally, they were washed twice with ethanol and dried at 70 °C in vacuum (10^{-3} mbar).

Wet-chemical deposition of Pt nanoparticles. The TiO_2–CeO_2–Pt_{WCD} hollow nanospheres can be decorated with Pt nanoparticles (1 wt-%) via wet impregnation. To this concern, 5.8 mg of $Pt(Ac)_2$ were dissolved in acetone and dropped onto a dried powder sample of TiO_2–CeO_2 hollow nanospheres.

scCO_2 for impregnation with Pt nanoparticles. The SFRD process to obtain TiO_2–CeO_2–Pt_{SFRD} hollow nanospheres was performed at a temperature of 80 °C and a CO_2 pressure of 15.6 MPa. 3.5 mg of [Pt(Cod)Me_2] (97 %, Sigma-Aldrich) and 135 mg of TiO_2–CeO_2 hollow nanospheres were filled into two separate open recipients inside the high-pressure reactor with a volume of 50 mL. Gaseous CO_2 was filled into the reactor and heated to the desired temperature within less than 2 h (i.e. 1.5 to 2.0 h). Subsequently, the mixture was treated in scCO_2 at 80 °C and 15.6 MPa for 20 h. During this time, [Pt(Cod)Me_2] was dissolved in scCO_2, and molecular adsorption of the precursor on the substrate takes place. Afterwards, H_2 (12 mol-%) was added to the system, and the mixture was kept at constant pressure and temperature for additional 2 h. In this process step, [Pt(COD)Me_2] was reduced to elemental Pt while the organic ligands were transformed to 1,5-cyclooctane and methane. At the end of the experiment, the system was slowly depressurized and cooled to ambient conditions. More details regarding the SFRD process, the equipment and further experimental details can be found elsewhere.[16,17,29]

CO oxidation. Sieved catalyst powders (5 mg, 125–250 μm grain size) were deposited in quartz microreactors (Ø: 1.5 mm) with glass wool plugs in front and at the back of the catalyst bed. A gas mixture of 50 mL/min 1,000 ppm CO, 10 % O_2 in He was dosed over that catalyst bed at ambient pressure. This corresponds to weight hourly space velocity of 60,000 L g_{Pt}^{-1} h^{-1}. The temperature was varied between 50–500 °C with a heating/cooling rate of 5 °C/min. The outlet gas composition was analyzed with an FT-IR spectrometer (Multigas Analyzer™, MKS Instruments) combined with a mass spectrometer (Pfeiffer Vacuum).

Supporting Information

Details of the analytical techniques and equipment.

Acknowledgements

The authors acknowledge the Deutsche Forschungsgemeinschaft (DFG) for funding within the Collaborative Research Center 1441 *„Tracking the Active Site in Heterogeneous Catalysis for Emission Control (TrackAct)"* (Project-ID 426888090). Open Access funding enabled and organized by Projekt DEAL.

Conflict of Interests

The authors declare no conflict of interest.

Data Availability Statement

The data that support the findings of this study are available from the corresponding author upon reasonable request.

Keywords: Catalyst · ceria · CO oxidation · hollow nanospheres · titania

[1] R. W. McCabe, A. Trovarelli, *Appl. Catal. B* **2016**, *197*, 1.
[2] P. Li, X. Chen, Y. Li, J. W. Schwank, *Catal. Today* **2019**, *327*, 90–115.
[3] a) Y. Choi, S. K. Cha, H. Ha, S. Lee, H. K. Seo, J. Y. Lee, H. Y. Kim, S. O. Kim, W. C. Jung, *Nat. Nanotechnol.* **2019**, *14*, 245–251; b) J. Wang, X. Xiao, Y. Liu, K. Pan, H. Pang, S. Wei, *J. Mater. Chem. A* **2019**, *7*, 17675–17702; c) D. Zhao, Y. Pi, Q. Shao, Y. Feng, Y. Zhang, X. Huang, *ACS Nano* **2018**, *12*, 6245–6251.
[4] a) S. Ranganathan, V. Sieber, *Catal.* **2018**, *8*, 3791–37922; b) R. Dittmeyer, J.-D. Grunwaldt, A. Pashkova, *Catal. Today* **2015**, *248*, 149–159; c) J. K. Edwards, S. J. Freakley, R. J. Lewis, J. C. Pritchard, G. J. Hutchings, *Catal. Today* **2015**, *248*, 3–9.

[5] Y. W. Hartati, S. N. Topkaya, S. Gaffar, H. H. Bahti, A. E. Cetin, *RSC Adv.* **2021**, *11*, 16216–16235.
[6] a) F. Maurer, A. Gänzler, P. Lott, B. Betz, M. Votsmeier, S. Loridant, P. Vernoux, V. Murzin, B. Bornmann, R. Frahm, O. Deutschmann, M. Casapu, J.-D. Grunwaldt, *Indust. Engineer. Chem. Res.* **2021**, *60*, 6662–6675; b) Z. W. Chen, L. X. Chen, C. C. Yang, Q. Jiang, *J. Mater. Chem. A* **2019**, *7*, 3492–3515; c) G. C. Dhal, S. Dey, D. Mohan, R. Prasad, *Catal. Rev.* **2018**, *60*, 437–496.
[7] a) F. Maurer, J. Jelic, J. Wang, A. Gänzler, P. Dolcet, C. Wöll, Y. Wang, F. Studt, M. Casapu, J.-D. Grunwaldt, *Nature Catalysis* **2020**, *3*, 824–833; b) M. Yashima, *Catal. Today* **2015**, *253*, 3–19; c) H. L. Tuller, *Solid State Ionics* **2000**, *131*, 143–157.
[8] a) D. Devaiah, L. H. Reddy, S.-E. Park, B. M. Reddy, *Catal. Rev.* **2018**, *60*, 177–277; b) D. M. Lyons, K. M. Ryan, M. A. Morris, *J. Mater. Chem.* **2002**, *12*, 1207–1212.
[9] a) S. Wolf, C. Feldmann, *Angew. Chem. Int. Ed.* **2016**, *55*, 15728–15752; b) Z. W. Shan, G. Adesso, A. Cabot, M. P. Sherburne, S. A. Syed Asif, O. L. Warren, D. C. Chrzan, A. M. Minor, A. P. Alivisatos, *Nat. Mater.* **2008**, *7*, 947–952.
[10] a) M. Liang, T. Borjigin, Y. Zhang, B. Liu, H. Liu, H. Guo, *Appl. Catal. B* **2019**, *243*, 566–575; b) W. Zhang, L.-P. Yang, Z.-X. Wu, J.-Y. Piao, A.-M. Cao, L.-J. Wan, *Chem. Commun.* **2016**, *52*, 1420–1423; c) M. Huang, Y. Zhang, Y. Zhou, C. Zhang, S. Zhao, J. Fang, Y. Gao, X. Sheng, *New J. Chem.* **2017**, *41*, 13472–13482; d) L. Liu, X. Yan, Y. Zhang, D. Deng, H. He, Y. Lei, X. Shen, L. Luo, *ACS Appl. Nano Mater.* **2023**, *6*, 2116–2124; e) Y. Liao, Y. Li, L. Wang, Y. Zhao, D. Ma, B. Wang, Y. Wan, S. Zhong, *Dalton Trans.* **2017**, *46*, 1634–1644; f) P. Shao, J. Tian, W. Shi, Y. Yang, X. Yang, S. Gao, F. Cui, *J. Mater. Chem. A* **2017**, *5*, 124–132.
[11] a) S. Cao, B. Zou, J. Yang, J. Wang, H. Feng, *ACS Appl. Nano Mater.* **2022**, *5*, 11689–11698; b) X. Wang, K. Fu, X. Wen, S. Qi, G. Tong, X. Wang, W. Wu, *Appl. Surf. Sci.* **2022**, *598*, 153826; c) M. Guzman, M. Estrada, S. Miridonov, A. Simakov, *Microporous Mesoporous Mater.* **2019**, *278*, 241–250; d) W. Liu, X. Liu, L. Feng, J. Guo, A. Xie, S. Wang, J. Zhang, Y. Yang, *Nanoscale* **2014**, *6*, 10693–10700.
[12] a) W. Wu, W. Qi, Y. Zhao, X. Tang, Y. Qiu, D. Su, H. Fan, G. Wang, *Appl. Surf. Sci.* **2019**, *463*, 244–252; b) W. Qi, W. Jiang, F. Xu, J. Jia, C. Yang, B. Cao, *Chem. Eng. J.* **2020**, *382*, 122852; c) X.-P. Fu, W.-Z. Yu, M.-Y. Li, R. Si, C. Ma, C.-J. Jia, *Inorg. Chem.* **2021**, *60*, 5183–5189; d) Q. Gong, T. Gao, H. Huang, R. Wang, P. Cao, G. Zhou, *Inorg. Chem. Front.* **2018**, *5*, 3197–3204.
[13] M. Liebertseder, D. Wang, G. Cavusoglu, M. Casapu, S. Wang, S. Behrens, C. Kübel, J.-D. Grunwaldt, C. Feldmann, *Nanoscale* **2021**, *13*, 2005–2011.
[14] D. Bartenbach, O. Wenzel, R. Popescu, L.-P. Faden, A. Reiß, M. Kaiser, A. Zimina, J.-D. Grunwaldt, D. Gerthsen, C. Feldmann, *Angew. Chem. Int. Ed.* **2021**, *60*, 17373–17377.
[15] C. Xie, Z. Niu, D. Kim, M. Li, P. Yang, *Chem. Rev.* **2020**, *120*, 1184–1249.
[16] M. Türk, C. Erkey, *J. Supercrit. Fluids* **2018**, *134*, 176–183.
[17] M. Türk, M. Crone, G. Upper, *J. Supercrit. Fluids* **2011**, *58*, 1–6.
[18] A. Galarneau, F. Villemot, J. Rodriguez, F. Fajula, B. Coasne, *Langmuir* **2014**, *30*, 13266–13274.
[19] M. Daturi, E. Finocchio, C. Binet, J.-C. Lavalley, F. Fally, V. Perrichon, H. Vidal, N. Hickey, J. Kaspar, *J. Phys. Chem. B* **2000**, *104*, 9186–9194.
[20] X.-D. Zhou, W. Huebner, H. U. Anderson, *Chem. Mater.* **2003**, *15*, 378–382.
[21] A. Bumajdad, M. I. Zaki, J. Eastoe, L. Pasupulety, *Langmuir* **2004**, *20*, 11223–11233.
[22] A. M. Gänzler, B. Betz, S. Baier-Stegmaier, S. Belin, V. Briois, M. Votsmeier, M. Casapu, *J. Phys. Chem. Chem. Phys. C* **2020**, *124*, 20090–20100.
[23] A. M. Gänzler, M. Casapu, D. E. Doronkin, F. Maurer, P. Lott, P. Glatzel, M. Votsmeier, O. Deutschmann, J.-D. Grunwaldt, *J. Phys. Chem. Lett.* **2019**, *10*, 7698–7705.
[24] L. Artiglia, F. Orlando, K. Roy, R. Kopelent, O. Safonova, M. Nachtegaal, T. Huthwelker, J. A. van Bokhoven, *J. Phys. Chem. Lett.* **2017**, *8*, 102–108.
[25] N. Bosio, M. Di, M. Skoglundh, P.-A. Carlsson, H. Grönbeck, *J. Phys. Chem. C* **2022**, *126*, 16164–16171.
[26] M. Casapu, A. Fischer, A. M. Gänzler, R. Popescu, M. Crone, D. Gerthsen, M. Türk, J.-D. Grunwaldt, *ACS Catal.* **2017**, *7*, 343–355.
[27] M. Cargnello, J. J. Delgado Jaén, J. C. Hernández Garrido, K. Bakhmutsky, T. Montini, J. J. Calvino Gámez, R. J. Gorte, P. Fornasiero, *Science* **2012**, *337*, 713–717.
[28] M. Basato, A. Biffis, G. Martinati, C. Tubaro, A. Venzo, P. Ganis, F. Benetollo, *Inorg. Chim. Acta* **2003**, *355*, 399–403.
[29] C. Erkey, M. Türk, in *Synthesis of nanostructured materials in near and/or supercritical fluids*. 1st Ed., Elsevier, Amsterdam **2021**.

Manuscript received: October 25, 2023
Revised manuscript received: November 7, 2023
Accepted manuscript online: November 7, 2023
Version of record online: ■■, ■■

RESEARCH ARTICLE

TiO_2–CeO_2–Pt hollow nanospheres (1 wt-% Pt) are prepared via a one-pot, liquid-phase approach using NaCl templates (outer diameter: 140–180 nm, wall thickness: 30–40 nm, inner cavity: 80–100 nm, specific surface area: 210 m^2/g, Pt nanoparticles: 2–3 nm). The high-porosity material is exemplarily tested for CO oxidation and shows promising properties.

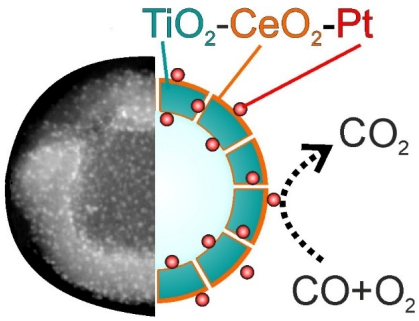

*Dr. M. Liebertseder, Dr. C. B. Maliakkal, M. Crone, Dr. G. Nails, Dr. M. Casapu, Prof. Dr. J.-D. Grunwaldt, Prof. Dr. M. Türk, Prof. Dr. C. Kübel, Prof. Dr. C. Feldmann**